Theory of thermal properties of magnetic materials with unknown entropy

Matthew Heine, Olle Hellman, and David Broido

Phys. Rev. Materials **6**, 113805 — Published 30 November 2022

DOI: 10.1103/PhysRevMaterials.6.113805

Theory of thermal properties of magnetic materials with unknown entropy

Matthew Heine,[1] Olle Hellman[2] and David Broido[1*]

[1]Department of Physics, Boston College, Chestnut Hill, Massachusetts 02467, USA

[2]Department of Materials and Interfaces, Weizmann Institute of Science, Rehovot 76100, Israel

Abstract-

Theoretical approaches to study thermal properties of magnetic materials typically require accurate models of magnetic interactions in order to define the entropy. Here we introduce a complementary approach for examining thermal properties in magnetic systems where an accepted model for such interactions does not exist. In place of a specific model for magnetic interactions, the approach integrates measurements of temperature dependent magnetization of the studied material into a first principles computational scheme. The approach calculates system pressure from thermally disordered microstates that properly incorporate vibrational and spin subsystems at each temperature as well as the coupling between these subsystems. We apply the approach to calculate phonon modes and to investigate the anomalously low thermal expansion of the classical Invar alloy, $Fe_{0.65}Ni_{0.35}$. The calculated phonon dispersions for Invar are in excellent agreement with measured data. The Invar thermal expansion is shown to remain small between 50 K and room temperature, consistent with the experimentally observed low thermal expansion value in this same temperature range. This anomalously small thermal expansion is directly connected to a small positive contribution from lattice thermal disorder that is nearly canceled by a large negative magnetic disorder contribution. By contrast, calculations for bcc Fe show a much larger thermal expansion, consistent with experiment, which is dominated by a large contribution from lattice thermal disorder that is reduced only slightly by a small negative contribution from that of

magnetism. These findings give insights into the unusual nature of magnetism and spin-lattice coupling in Invar and Fe. In addition, they give promising preliminary support to the presented new methodology as a complementary way to investigate thermal properties of magnetic materials. The success achieved on Invar and Fe motivates future testing of the approach on other magnetic materials.

* broido@bc.edu

I. Introduction

Theoretical approaches to calculate phonons and thermal properties start from the Helmholtz Free energy, $F = F(V,T) = E - TS$, where E is the energy, T is temperature, V is the crystal volume, and S is the entropy. At each T, the equilibrium volume, $V(T)$, is the one that makes the pressure, $P = -(\partial F/\partial V)_T$, vanish. Once it is obtained, thermal expansion can be assessed from the change in V with T along the curve $V(T, P = 0)$ i.e. the one for which P vanishes. Implementation of this theoretical approach requires an accurate model for F and hence the entropy. In a magnetic material, the latter has contributions from the vibrational and magnetic subsystems: $S = S_{vib} + S_{mag}$. In magnetic materials that have accepted theoretical models of magnetic interactions, phonon modes renormalized by both anharmonicity and magnetism as well as spin-lattice coupling can be obtained [1, 2], thus giving S_{vib}. Similarly, knowledge of magnetic interactions allows the construction of models for S_{mag}.

In the present work, we introduce a complementary *ab initio*-based theoretical approach to calculate phonons and to examine thermal properties such as thermal expansion in a magnetic material for which an accepted model for the magnetism does not exist. The theory bypasses the need to define the free energy. Instead, configurational averages over microstates of thermally disordered atomic displacements and magnetic moment orientations are connected to the measured temperature-dependent magnetization. Using this input from measurement, the approach extracts temperature dependent phonon modes renormalized by both anharmonicity and spin-lattice coupling. In addition, by identifying the $V(T)$ giving zero pressure at different T, the thermal expansion can be examined.

To test this theoretical approach, we apply it to calculate phonons and to examine thermal expansion in the "classical Invar" alloy, $Fe_{0.65}Ni_{0.35}$ [3], and in bcc Fe. It is well-known that Invar

possesses an anomalously low thermal expansion coefficient around and below room temperature, which is referred to as the Invar effect [4-7]. The explanation for the anomalous thermal expansion has been an open question in condensed matter physics for over a century [6, 8-12], and a complete theoretical description of this behavior is outside the scope of the present work. Nevertheless, we endeavor to assess the merits of the developed theory by (i) comparing calculated phonon dispersions to experiment and (ii) investigating the commonly held notion that the Invar effect arises from a near perfect cancellation between a positive contribution to thermal expansion by the vibrating lattice and a negative contribution from the magnetic subsystem [12].

Excellent agreement is obtained with the measured room temperature (RT) phonon dispersions in Invar, which, to our knowledge, has not been demonstrated before. Remarkably, the calculations also identify a near-zero thermal expansion for Invar in the range 50K to 300K, consistent with measurement. The findings suggest that the small thermal expansion in Invar results from a reduced contribution from thermal lattice disorder that is nearly canceled by a large negative contribution from thermal magnetic disorder.

To further test the developed theoretical approach, we have also performed calculations for bcc Fe. bcc Fe is a well-studied magnetic material for which accepted models of the magnetic interactions exist. It also has a relatively large thermal expansion coefficient. It therefore provides a useful contrasting case to that of Invar. Excellent agreement with the measured RT phonon dispersions of bcc Fe is obtained using the new approach. In contrast to Invar, a much larger thermal expansion is found for Fe, in an equivalent temperature range, whose value is consistent with experiment. For Fe, the lattice thermal disorder contribution to thermal expansion dominates while the analogous contribution from the magnetic subsystem is found to be small.

II. Thermal properties from configurational averaging of microstates

As noted above, a common theoretical approach to calculate phonons and thermal properties of a material such as thermal expansion involves determination of $V(T, P = 0)$ at each T, by first calculating the free energy, $F(V, T)$ and then determining where $P = -(\partial F/\partial V)_T$ vanishes. The Helmholtz free energy, $F = E - TS$, contains both vibrational and magnetic contributions. The present approach bypasses the need to explicitly define the entropy in the following way. First, we express F as: $F = -k_B T ln(Z(V, T))$, where $Z(V, T)$ is the partition function:

$$Z(V, T) = \sum_i exp(-E_i/k_B T) \quad (1)$$

where the sum over i is a sum over all microstates, and E_i is the energy of microstate i. Then,

$$P(V, T) = -\left(\frac{\partial F}{\partial V}\right)_T = \sum_i p_i \left(-\frac{\partial E_i}{\partial V}\right) = \langle (P_i) \rangle_{V,T} \quad (2)$$

where $p_i = exp(-E_i/k_B T)/Z$ is the probability of occurrence of microstate *i*, and in the last term in Eq. 2 the angle brackets < ... >$_{V,T}$ represent a configurational average over microstates in the canonical ensemble for a given V and T. Here, we have defined a microstate pressure: $P_i = -(\partial E_i/\partial V)$. We note that P_i is not a thermodynamic quantity but merely a notational convenience.

An important feature of using Eq. 2 is that it avoids dealing explicitly with the entropy. Entropy is not neglected; instead, it is dealt with implicitly through the configurational averaging. Conceptually, it may help to recall that entropy is a function of the microstate probability distribution, p_i, [13], $S = -k_B \sum_i p_i ln(p_i)$. Therefore, a choice of microstate averaging is effectively a choice of entropy.

We now discuss the computational approach to determine the microstates appropriate to each V, T and to identify which ones should be included in the configurational averaging.

III. Computational Approach

In order to calculate the pressure, $P(V, T)$, from Eq. 2, we need to obtain P_i values and perform the configurational averaging. Toward that end, our first step is to obtain the phonon modes. Then,

we discuss how to calculate the microstate energies and demonstrate how to organize these so as to extract $P(V,T)$. All calculations are implemented within the framework of Density Functional Theory (DFT), as implemented in VASP [14-17]. These calculations employed the projector augmented wave method [18, 19] and the generalized gradient approximation as parametrized by Perdew Burke and Ernzerhof [20] to treat the exchange correlation functional. A 4x4x4 k-point grid was used along with a plane wave energy cutoff of 400eV. Spin-orbit coupling along with fully noncollinear magnetism was used, with moment directions constrained according to the spin-lattice snapshots. [19, 21].

Phonons: To calculate phonon modes, we use the temperature dependent effective potential (TDEP) scheme [1, 2, 22]. In the TDEP approach, a set of supercell "snapshots", each possessing thermally relevant atomic displacements and magnetic moment orientations, is generated for a set of $\{V, T\}$. In the present work, this is achieved using a stochastic sampling approach [23-25]. Here we use a 32-atom supercell. In principle, the chemical disorder of this random alloy may be treated in the same fashion, but for computational efficiency, the technique of special quasi-random structures (SQS) is used [26] to populate the supercell with Fe and Ni atoms in the proper proportion, as has be done previously with TDEP [27]. The SQS were initiated from a spherically random distribution of spin orientations. We used Metropolis Monte-Carlo to optimize the spin-spin correlation functions. We considered spin correlations between pairs of atoms up to four neighbors, weighted inversely with distance. We used a single SQS configuration as the starting point and then created multiple spin-lattice snapshots by generating many different thermal atomic and moment configurations for that same underlying SQS structure. For each pressure, P_i, in Eq. 2, 50 spin-lattice snapshots were found to be sufficient, as detailed in Appendix A. The phonon dispersions were also calculated from 50 spin-lattice configurations. Note that all atoms are

thermally displaced, the magnetic moments are thermally disordered, and some atoms are Fe while others are Ni, according to the SQS calculation. A DFT calculation is then performed for each of these thermally and chemically disordered supercell snapshots in order to interrogate the interatomic potential energy surface by generating force-displacement relationships for the atoms. Figure 1 shows a schematic of the range of thermally disordered moment orientations for Invar.

The TDEP Hamiltonian is

$$H_{TDEP} = U_0 + \sum_{i,\alpha} \frac{P_{i,\alpha}^2}{2M_i} + \frac{1}{2} \sum_{i,j,\alpha,\beta} \Phi_{i,j}^{\alpha,\beta}(V,T)\, u_{i,\alpha} u_{j,\beta} \qquad (3)$$

where U_0 is the equilibrium energy, M_i is the mass of atom i, $P_{i,\alpha}$ and $u_{i,\alpha}$ are the corresponding momentum and displacement along the Cartesian direction, α ($\alpha = x, y, z$), and $\Phi_{i,j}^{\alpha,\beta}(V,T)$ are effective interatomic force constants (IFCs) which are explicit functions of both V and T. Any number of IFCs may be used in our framework. For each (V-T), the effective IFCs are defined to be those that best reproduce, in the least-squares sense, the ensemble of thermally-relevant DFT-calculated force-displacement relationships described above. Thus these effective IFCs best reproduce the thermally-sampled Born-Oppenheimer (BO) energy surface, contrasted with frequently-constructed IFCs which are derivatives of the BO energy surface with respect to a static ideal lattice.

In this way, effects of spin-lattice coupling are captured *implicitly*; the effective IFCs are those that best reproduce *all* the effects present in the DFT calculations, including spin-lattice coupling as well as lattice anharmonicity, chemical disorder, and local environment effects. The end output

of the calculation is therefore a monatomic fcc lattice of an effective atom with renormalized IFCs and renormalized phonon modes are calculated by diagonalizing the dynamical matrix.

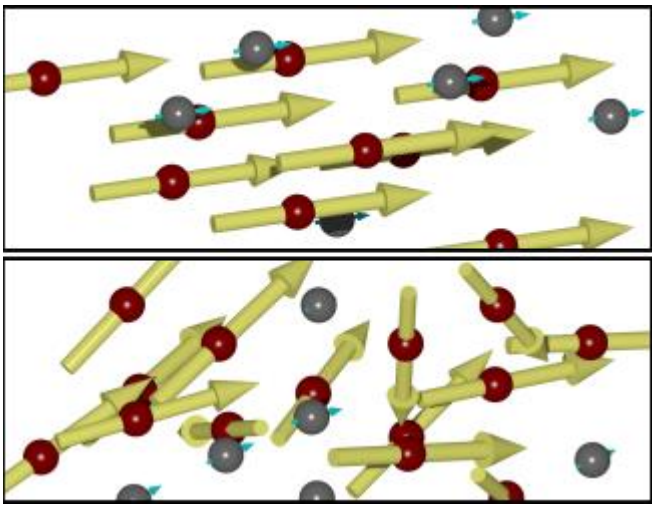

FIG. 1. Example of thermal spin-lattice snapshots (microstates) for the Invar calculation. Spheres represent Fe (red) and Ni (grey) atoms while arrows represent corresponding magnetic moments. Top and bottom panels show ferromagnetic and room-temperature arrangements, respectively.

Calculation of microstates: For each spin-lattice snapshot, i, a DFT calculation gives us an energy, $E_{DFT}[i]$. However, since the atoms in such a snapshot are thermally displaced but still stationary, this calculation neglects the kinetic energy of the ions. In actuality, each microstate energy is given by: $E_i = K_i + E_{DFT}[i]$, where K_i is the ion kinetic energy of microstate i. In principle, the kinetic energy contribution could be obtained in a molecular dynamics (MD) calculation, but such a calculation would omit important quantum mechanical behavior. In particular, at low temperatures, zero-point motion can dominate the amplitudes of the atomic displacements. The zero-point motion is captured within our snapshots approach. Also, the time evolution of the noncollinear magnetic moments within such an MD calculation is a nontrivial problem to solve.

The thermodynamic pressure can then be expressed as:

$$P(V,T) = P^K(V,T) + \langle P_{DFT}[i] \rangle_{V,T} \tag{4}$$

where the first term is the contribution to pressure from the ion kinetic energy and the second term is the remaining contribution extracted from the DFT calculations: $\langle P_{DFT}[i] \rangle_{V,T} = \langle -\partial E_{DFT}[i]/\partial V \rangle_{V,T}$. In the quasi-harmonic approximation, it is straightforward to show that [28]:

$$P^K(V,T) = \frac{1}{2} P^{vib}(V,T) \tag{5}$$

where P^{vib} is the contribution to the pressure from the vibrational energy, E^{vib}. It can be obtained in a straightforward way once the relevant microstates are identified.

The configurational averaging over magnetic states could also be accomplished if a theory describing magnetism in the material of interest were known. For example, in Fe the magnetic system is often described theoretically using the Heisenberg model. We have found excellent agreement with the measured temperature dependent phonon frequencies using the Heisenberg model within the TDEP framework [1]. The present approach is developed for cases where an accepted theory of the magnetic interactions does not exist. The theory proceeds by integrating experimental measurements of the normalized magnetization as a function of temperature to guide the selection of microstates to be used in the configurational averaging. A central finding of the present work is that, for both bcc Fe and Invar, the calculated total pressure can be directly specified by the normalized magnetization. Moreover, we find that configurational averaging over magnetic states is unnecessary; using a single magnetic "snapshot" consistent with measurement is sufficient for calculating pressure.

Each magnetic snapshot may be characterized by a normalized magnetization, $\mathfrak{M}$, defined as the net magnetization per atom of the supercell divided by the average local moment size. The total pressure is taken to be the pressure calculated using a single magnetic snapshot of normalized magnetization, $\mathfrak{M}$:

$$P(V,T) \approx P_{\mathfrak{M}}(V,T) \tag{6}$$

In the calculation of $P_{\mathfrak{M}}$, averaging over various thermally-displaced atomic configurations is still performed, but only a single magnetic configuration is used. This approximation was validated by demonstrating that pressures derived from considering only one magnetic state according to Eq. 6 were equivalent to the pressure calculated when averaging over magnetic states with similar $\mathfrak{M}$.

A detailed description of this computational scheme and its justification for Invar are presented in Appendix A.

IV. Results

To our knowledge, an *ab initio* calculation of phonon dispersions in $Fe_{0.65}Ni_{0.35}$ and demonstrated agreement with this measured data does not exist. Figure 2 shows the calculated room-temperature (296K) phonon dispersions using the presented computational approach compared to measured data at that same temperature [29-31]. Calculations are for a lattice constant of a = 3.5845Å, which was found to give nearly zero pressure at room temperature, and a normalized magnetization value of $\mathfrak{M} = 0.8$, consistent with the measured lattice constant [32] and magnetization of the Invar alloy [33-36] at room temperature. The excellent agreement with measured data supports the employed strategy of using a magnetic configuration with $\mathfrak{M}$ closest to the measured normalized magnetization value.

We have tested the sensitivity of phonons to independent changes of magnetization, volume, and temperature. We find that (i) holding T and V fixed, increased magnetic disorder produces an overall softening of phonon modes, and (ii) holding T and $\mathfrak{M}$ fixed, decreasing V stiffens phonon modes. Interestingly, upon performing calculations at T = $0K$, $50K$, $300K$, and $600K$, but keeping the magnetic configuration and volume fixed, the phonon dispersions were found to be nearly independent of T. Thus, the phonons are insensitive to larger atomic displacements

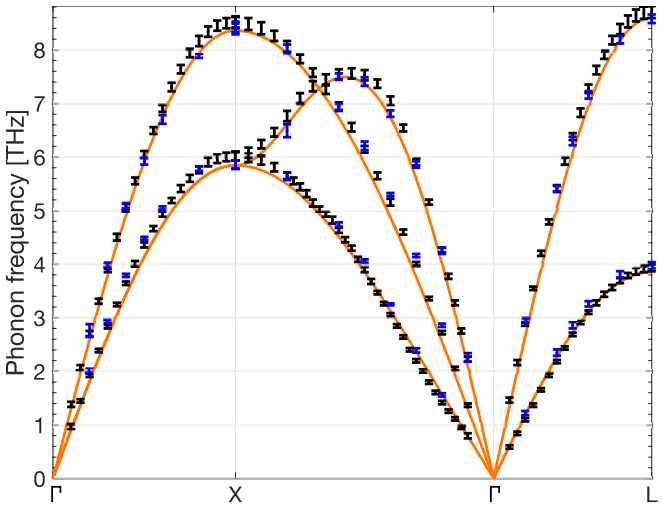

FIG. 2. Calculated phonon dispersions for the classical Invar alloy at room temperature compared to measurement. Blue error bars are measurements of $Fe_{0.7}Ni_{0.3}$ from Ref. 30 while black error bars are measured data for $Fe_{0.65}Ni_{0.35}$ from Ref. 31.

produced by increasing temperature when V and $\mathfrak{M}$ are held fixed. This points to possible weak anharmonicity in the Invar bonding since the larger displacement amplitudes with increasing T cause the constituent atoms to sample more anharmonic parts of the chemical bonds, but in Invar, this does not in itself significantly renormalize the phonon modes. In contrast, we have found that for bcc Fe, the increase in lattice thermal atomic displacement amplitudes produced significant renormalization of the phonon modes [1].

Figure 3 investigates the effects of changing lattice thermal disorder and magnetic thermal disorder independently. It compares the calculated pressures, $P_{\mathfrak{M}}$, for Invar (left panel) and bcc Fe (right panel) for two different lattice temperatures. The color of each circle shown corresponds to a particular normalized magnetization spanning ferromagnetic ($\mathfrak{M} = 1$; yellow circles) to paramagnetic ($\mathfrak{M} = 0$; blue circles), as conveyed in the colorbar on the right. For Invar, the two temperatures chosen are 50K and 296K, while for bcc Fe they are 300K and 600K. These temperatures reflect low and medium values relative to the respective transition temperatures of around 500K and 1043K. The same lattice constants for Invar (3.5845Å) and Fe (2.83Å) are used at each of the two temperatures, and these lattice constants are chosen to give roughly zero pressure at the lower of the two temperature values for the points matching the measured magnetizations at those temperatures. We note that these lattice constant values are in good agreement with measured values [32, 37].

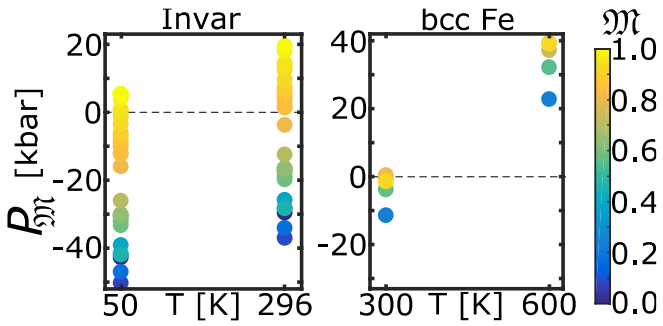

FIG. 3. Left panel: Calculated $P_{\mathfrak{M}}$ for Invar at ambient volume for T=50K and normalized magnetization, $\mathfrak{M}$, ranging from ferromagnetic, $\mathfrak{M}$=1, to paramagnetic, $\mathfrak{M}$=0 (see colorbar for normalized magnetization scale). Calculated $P_{\mathfrak{M}}$ values at T=296K use the ambient volume at 50K. Right panel: Same for bcc Fe for T=300K and T=600K.

The figure demonstrates the relative effects of lattice and magnetic thermal

disorder on contributions to pressure in Invar compared with those for bcc Fe as the temperature is changed. A positive change in pressure in going from the lower to the higher temperature works to expand the crystal (increase the lattice constant) while a negative change in pressure works to contract the lattice (decrease the lattice constant). From this plot, we can make several conclusions. First, it is apparent that, in both Invar and bcc Fe, increasing magnetic disorder at a given temperature (i.e. decreasing $\mathfrak{M}$ so moving from yellow circles towards blue circles) lowers the pressure (i.e. corresponds to moving vertically downward). Thus, the magnetic thermal disorder acts to reduce the lattice constant corresponding to a negative contribution to thermal expansion. Second, the magnitude of this effect is significantly larger in Invar than it is in bcc Fe. Specifically, comparing the spreads of the pressure ranges between fully-aligned ferromagnetic (yellow) to random paramagnetic (blue) shows that this range is much larger in Invar than it is in bcc Fe. Thus, the same increase in magnetic thermal disorder produces a larger negative contribution to the thermal expansion in Invar than is the case for bcc Fe. Third, note the relative shift of each vertical set of points between the two temperatures for each material. Comparing points of equivalent magnetization at the two temperatures represents the effect of the lattice thermal disorder on pressure: an increase in pressure with increasing temperature corresponds to positive thermal expansion (i.e. the lattice wants to expand to reduce the pressure back to zero). The smaller pressure differences evident in Invar show that the contribution to its thermal expansion from increasing thermal lattice disorder is suppressed compared with bcc Fe.

Figure 4 plots the $P_{\mathfrak{M}}$ values for Invar (left panel) and bcc Fe (right panel) for a subset of the magnetizations shown in Fig. 3. The point marked "a" in the left panel corresponds to the zero pressure point for Invar at 50K, obtained for the lattice constant, 3.5845Å and a magnetization value of $\mathfrak{M} = 0.95$, consistent with corresponding measured values [32, 33]. The point marked

"c" is calculated using the same 50K lattice constant, but now using thermal lattice configurations for 296K and the measured room temperature magnetization value of around $\mathfrak{M} = 0.8$. The small value of P found at point c (296K) is consistent with a near-zero thermal expansion over the 50K-300K range [38].

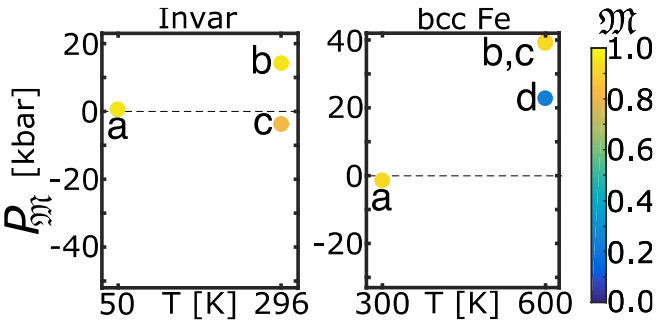

FIG. 4. Calculated $P_{\mathfrak{M}}$ for a subset of values in Fig. 3, for Invar (left panel) and for bcc Fe (right panel). See Fig. 3 caption for axes/colormap definitions. Labeled points for Invar are: point a: $P_{\mathfrak{M}}(T = 50\text{K})$ using $\mathfrak{M}$ consistent with measured magnetization at 50K; point b: $P_{\mathfrak{M}}(T = 296K)$ for same $\mathfrak{M}$ as at 50K. point c: $P_{\mathfrak{M}}(T = 296K)$ with $\mathfrak{M}$ consistent with measurement at 296K; Labeled points a, b, c for bcc Fe have same meaning as corresponding points for Invar but at 300K and 600K. Point d: $P_{\mathfrak{M}}$ for a paramagnetic configuration.

The lack of thermal expansion in Invar is found to be a consequence of a cancellation between the positive contribution from the lattice thermal disorder and the negative contribution from that of magnetism, as has been postulated before. This can be seen as follows. Starting at $P(T = 50K)$ (point a) and increasing T to 296K while keeping the normalized magnetization, $\mathfrak{M}$, fixed at the 50K value brings us to point b. In this move from a to b, the only change is that lattice thermal disorder has increased. Thus, the increase seen in $P_{\mathfrak{M}}$ upon moving from a to b is caused by the increase in thermal lattice disorder. This is the normal positive thermal expansion behavior driven by lattice anharmonicity: the lattice must expand to reduce the pressure at point b to zero. But in reality, $\mathfrak{M}$ also decreases when T is increased, as the magnetic moments become more thermally disordered. Including this disorder by reducing $\mathfrak{M}$ to match the measured value at 296K reduces the pressure to the near-zero value at point c. Thus, for Invar, the negative contribution to thermal expansion from the increased thermal magnetic disorder is found to almost exactly cancel the positive contribution from the increased thermal lattice disorder.

The results of similar calculations for bcc Fe are shown in the right panel of Fig. 4. In contrast to the findings in Invar, bcc Fe shows a large positive thermal expansion: point c is at a much higher pressure than point a, indicating that the zero-pressure volume for T=600K is noticeably larger than that for T=300K. This large increase is consistent with the measured large thermal expansion coefficient in bcc Fe [39]. It is dominated by the contribution from lattice thermal disorder, which can be seen by moving from point a to point b (increasing T at fixed V and $\mathfrak{M}$), which causes only a slightly larger increase in pressure (not visible on figure) compared with the move from a to c. Thus, we conclude that the contribution to thermal expansion from lattice thermal disorder is much larger in bcc Fe than in Invar. Furthermore, since the move from b to c in bcc Fe is quite small, we conclude that the negative contribution to thermal expansion in Fe from increasing magnetic disorder is negligible in this temperature region. In fact, even increasing magnetic disorder in Fe to the fully-random paramagnetic extreme (point d) would not reduce the pressure enough to make the bcc Fe result consistent with zero thermal expansion.

The anomalously small thermal expansion in Invar has been described in terms of a magneto-volume effect: the reduction in magnetization from the added thermal disorder with increasing temperature drives a decrease in volume that counteracts the normal positive thermal expansion due to anharmonicity. The present findings add to this general picture in the following ways: (i) The sensitivity of pressure to magnetization (Fig. 3a) and in particular, the large b-to-c pressure decrease (Fig. 4a) in Invar demonstrates the large magneto-volume effect. Broadly, we can connect this behavior to the spin-lattice coupling: more spin disorder acts to push the lattice atoms closer together; (ii) The relatively small increase in pressure upon increasing temperature for fixed magnetization and volume (i.e. going from point a to point b in Fig. 4a) gives evidence for possible weak anharmonicity. Such weak anharmonicity was already noted above in connection with the

relative independence of the Invar phonon frequencies to changes in temperature for fixed volume and magnetization. The corresponding small a-to-b pressure increase means that a smaller magneto-volume contraction is needed to achieve zero thermal expansion; (iii) The contrast between the Invar behavior and that found in bcc Fe is striking: bcc Fe shows both stronger anharmonicity and a much weaker negative magneto-volume effect. The latter reflects in part underlying differences in the nature of the magnetic interactions in Invar compared with bcc Fe. For example, using a Heisenberg model with constant exchange integral for spin-spin interactions would give $P_{\mathfrak{M}}$ that are independent of the magnetization. The near-independence of $P_{\mathfrak{M}}$ on magnetization seen in Fig. 3b for bcc Fe is consistent with it having been often described by such a Heisenberg model, which also captures reasonably well its temperature dependent magnetization. In contrast, the strong dependence of $P_{\mathfrak{M}}$ on magnetization seen in Invar (Fig. 3a), suggests that a more exotic model of magnetic interaction would be more appropriate for Invar. We note that the measured temperature dependence of the Invar magnetization [40] supports this, as it does not fit the Heisenberg model's Brillouin magnetization curve, decreasing more rapidly at low T and more slowly for $T \sim T_c$.

V. Conclusions

In summary, a first principles-based theoretical framework for calculating temperature dependent phonons and examining thermal properties in magnetic materials of unknown entropy was presented. The approach integrates experimental measurements of the normalized magnetization into *ab initio* calculations of thermodynamic pressure in terms of configurational averaging over spin-lattice microstates. In this approach, the entropy is thus incorporated *implicitly* rather than explicitly. Thermal disorder in lattice and magnetic subsystems as well as spin-lattice coupling effects are naturally captured.

The approach was tested on the classical Invar alloy $Fe_{0.65}Ni_{0.35}$ and on bcc Fe. Excellent agreement with the measured room temperature phonon dispersions of Invar was achieved which, to our knowledge, has not been demonstrated previously. The results give a picture of the Invar effect in which (i) the positive contribution to thermal expansion from thermal lattice disorder is relatively small, possibly because of weak bond anharmonicity; (ii) a negative contribution to thermal expansion occurs from magnetic thermal disorder that is relatively large in magnitude. The combination gives a near perfect cancellation between lattice and magnetic contributions to the thermal expansion in Invar. The behavior in bcc Fe is found to be in striking contrast, where a large positive lattice contribution to thermal expansion is hardly reduced by the small magnetic negative contribution. These findings are qualitatively consistent with prior predictions and measurements. It is striking that this remarkable combination of contrasting results, is captured using finite-temperature *ab initio* calculations within the DFT framework.

We note that the new approach can in principle accommodate magnetic materials with more complex crystal structures and those containing heavy atoms where inclusion of spin-orbit coupling is essential. Increasing the number of atoms in the unit cell may require use of larger supercells, which would increase the computational cost. As long as the phonon and magnetic subsystems can be accurately described within the framework of density functional theory, we would expect that the approach should properly describe phonons and thermal properties.

It would be interesting to implement the new approach to investigate other magnetic systems with exotic magnetic interactions. For example, can the DFT-based approach accurately describe phonons and thermal properties of magnetic materials with large Dzyaloshinskii–Moriya interactions? Such an examination may be possible in two-dimensional magnets where larger supercells comparable to the size of spin textures may be computationally accessible. Since the

new computational scheme relies on incorporating the measured temperature dependent magnetization in order to determine the thermally disordered spin configurations, such data would have to be available.

We emphasize that the results presented for thermal expansion in Invar and Fe are somewhat qualitative, and we do not claim to give a deep theoretical explanation for the anomalously small thermal expansion in Invar. Nevertheless, the proper trends that are identified along with the excellent agreement of the calculated phonon dispersions of Invar compared to experiment suggest that the new method may be a fruitful path for *ab initio* study of the thermal properties of magnetic materials of unknown entropy at finite temperature, which deserves further investigation. In particular, it would be useful to study more magnetic materials to identify boundaries of validity of the developed theory. Among possible materials systems to study are other Invar alloys, and materials with complex correlated magnetic behavior, such as those involving the Dzyaloshinskii–Moriya interactions mentioned above. From such studies, it may be possible to extract useful information about the magnetic interactions, which would aid in developing appropriate theoretical models.

Acknowledgements: This work was supported by the U.S. Department of Energy, Office of Science, Basic Energy Sciences, under Award # DE-SC0021071. M. H. and D. B. also acknowledge computational support from the Boston College Linux Cluster.

Appendix A: Connecting configurational averaging to measured magnetization

The microstates i.e. spin-lattice snapshots, enumerated by index i, are decomposed into $i = (\mathcal{L}, \mathcal{M})$, where $\mathcal{L}$ labels each lattice configuration, i.e. snapshot of atomic displacements, and $\mathcal{M}$ labels each magnetic configuration i.e. snapshot of magnetic moment orientations. Then, the configurational averaging to determine the DFT pressure, $\langle P_{DFT}[i]\rangle_{V,T}$, from Eq. 4, can be written:

$$\langle P_{DFT}[i]\rangle_{V,T} = \sum_{\mathcal{M}} \sum_{\mathcal{L}} w_{\mathcal{M}} w_{\mathcal{L}} P_{DFT}[(\mathcal{M}, \mathcal{L})] \tag{A1}$$

where $w_{\mathcal{M}}$ and $w_{\mathcal{L}}$ are the statistical weights of each magnetic and lattice state, respectively. By construction, each generated lattice configuration is an equally probable one for each (V, T) so $w_{\mathcal{L}} = 1/N_{\mathcal{L}}$, where $N_{\mathcal{L}}$ is the total number of lattice configurations considered. In our calculations, we performed the average over $\mathcal{L}$ first. For a given $\mathcal{M}$, we found the average $\sum_{\mathcal{L}} w_{\mathcal{L}} P_{DFT}[(\mathcal{M}, \mathcal{L})]$ to be well-converged (within ± 0.5 kbar) using 25 different lattice configurations. The calculations in this manuscript employ 50 lattice configurations for each $P_{\mathcal{M}}$ value. A single SQS supercell was used.

To identify the appropriate set of magnetic microstates, we start by defining a "pressure" for a given magnetic configuration, $\mathcal{M}$, as $P_{\mathcal{M}}$, such that

$$P_{\mathcal{M}}(V,T) = \frac{1}{2} P_{vib}(V,T) + \frac{1}{N_{\mathcal{L}}} \sum_{\mathcal{L}} P_{DFT}[(\mathcal{M}, \mathcal{L})] \tag{A2}$$

Then, the total pressure is:

$$P(V,T) = \sum_{\mathcal{M}} w_{\mathcal{M}} P_{\mathcal{M}}(V,T) \tag{A3}$$

To gain insight about how to group the magnetic states, the supercell atoms were placed at their equilibrium positions. Ideal lattice positions were used here rather than performing a magnetic relaxation for each thermally-displaced atomic configuration at each volume and temperature due to the high computational cost of such calculations. Then, various paramagnetic (fully random moment orientations) starting moment configurations were generated, and these were allowed to

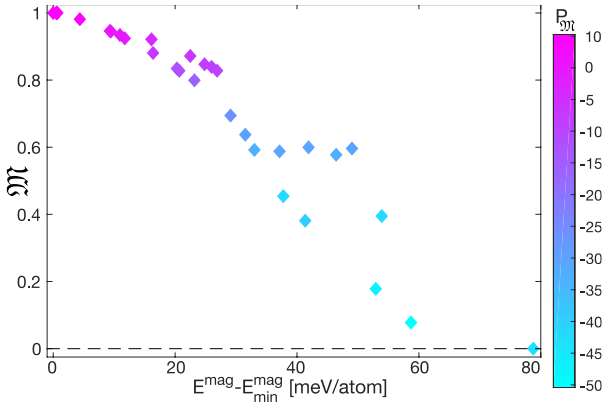

FIG 5. Dependence of $P_{\mathcal{M}}$ for Invar upon degree of disorder, $\mathfrak{M}$, and energy of the magnetic state. Values of $P_{\mathcal{M}}$ are given by color (see colorbar for values in kbar). E^{mag} is the energy of the given magnetic configuration with atoms in the ideal lattice positions; E_{min}^{mag} is the lowest energy of the plotted configurations. All points correspond to a lattice temperature of 50K.

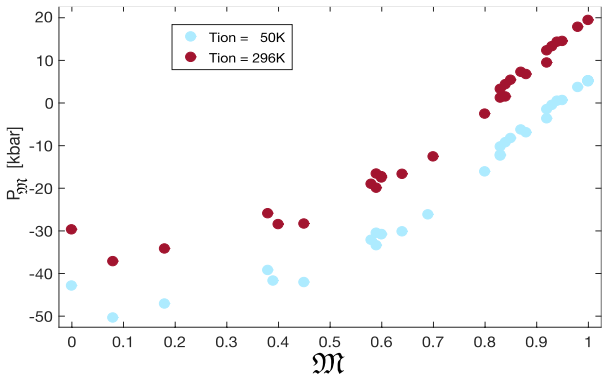

FIG. 6. Dependency of $P_{\mathcal{M}}$ for Invar on degree of magnetic disorder, $\mathfrak{M}$ for lattice temperatures of 50K and 296K. The T=50K data is the same as in Fig. 5. For the $\mathfrak{M}$ range of interest, $P_{\mathcal{M}}$ is a well-determined linear function of $\mathfrak{M}$.

energetically relax towards the ground state, which was found to be ferromagnetic for both Invar and Fe. From the intermediate states visited during these magnetic relaxations, we extract a subset composing the set $\{\mathcal{M}\}$. Each $\mathcal{M}$ is characterized according to their normalized magnetizations, $\mathfrak{M}$, and their energy above the ground state. Fig. 5 plots the dependency of $P_{\mathcal{M}}$ (for a representative subset of $\mathcal{M}$) on amount of magnetic order, $\mathfrak{M}$, and energy above the ground state. From this figure can be seen the important conclusion that $P_{\mathcal{M}}$ is determined exclusively by $\mathfrak{M}$ and is virtually independent of energy. This is seen by the fact that the color is essentially determined by the vertical position of a point on the plot and is unaffected by horizontal location. Analogous behavior was observed for $T = 296K$. Fig. 6 plots the same data (with the addition of $T = 296K$ data) without any designation of energy. The conclusion from Fig. 5 can also be seen in this figure in that the vertical spread (different energies) of points with similar $\mathfrak{M}$ is small. This demonstrates that, for the purpose of calculating pressure, the relevant characteristic of magnetic disorder for a microstate is $\mathfrak{M}$, the amount of orientational disorder in the magnetic moments. Furthermore, Fig.

6 demonstrates that, for the $\mathfrak{M}$ values of interest in this study, $P_{\mathcal{M}}$ is a simple *linear* function of $\mathfrak{M}$.

References

[1] Matthew Heine, Olle Hellman, and David Broido. Effect of thermal lattice and magnetic disorder on phonons in bcc Fe: A first-principles study. Phys. Rev. B 100, 104304 (2019).

[2] Matthew Heine, Olle Hellman, and David Broido, Temperature-dependent renormalization of magnetic interactions by thermal, magnetic, and lattice disorder from first principles, Phys. Rev. B 103, 184409 (2021).

[3] The standard composition of Invar alloy is Fe:64% and Ni:36%. For the calculations, we have used Fe:65% and Ni:35%, for which near zero thermal expansion has also been measured.

[4] Ch. E. Guillaume, Recherches sur les aciers au nickel. Dilatations aux temperatures elevees; resistance electrique," C.R. Acad. Sci. 125, 235 (1897).

[5] C. E. Guillaume, Nobel Lecture: Invar and Elinvar, Nobel Media AB, 2014, http://www.nobelprize.org/nobel_prizes/physics/laureates/1920/guillaume-lecture.html [or C. E. Guillaume, Nobel Lectures in Physics 1901–1921 (Elsevier, Amsterdam, 1967)].

[6] R.J. Weiss, The origin of the 'Invar' Effect, Proc. Phys. Soc. 82, 281 (1963).

[7] E.F. Wasserman, The Invar problem," J. Magn. Magn. Mater. 100, 346 (1991).

[8] Y. Kakehashi, Theory of the Invar Effect in FeNi Alloy, J. Phys. Soc. Jpn. 50, 2236 (1981).

[9] M. van Schilfgaarde, I. A. Abrikosov, and B. Johansson, Origin of the Invar effect in iron-nickel alloys, Nature 400, 46 (1999).

[10] V. Crisan, P. Entel, H. Ebert, H. Akai, D. D. Johnson, and J. B. Staunton, Magnetochemical origin for Invar anomalies in iron-nickel alloys, Phys. Rev. B 66, 014416 (2002).

[11] A. V. Ruban, S. Khmelevskyi, P. Mohn, and B. Johansson, Magnetic state, magnetovolume effects, and atomic order in Fe65Ni35 Invar alloy: A first principles study, Phys. Rev. B 76, 014420 (2007).

[12] A. Ruban, First-principles modeling of the Invar effect in $Fe_{65}Ni_{35}$ by the spin-wave method, Phys. Rev. B 95, 174432 (2017).

[13] R. K Pathria and Paul D Beale. Statistical mechanics, 3rd Edition. Elsevier Academic Press, Amsterdam, 2011.

[14] G. Kresse and J. Hafner, Efficient iterative schemes for ab initio total-energy calculations using a plane-wave basis set, Phys. Rev. B 48, 13115 (1993).

[15] G. Kresse and Furthmüller, Efficiency of ab-initio total energy calculations for metals and semiconductors using a plane-wave basis set, Comput. Mater. Sci. 6, 15 (1996).

[16] G. Kresse and D. Joubert, Efficient iterative schemes for ab initio total-energy calculations using a plane-wave basis set, Phys. Rev. B 54, 11169 (1996).

[17] G. Kresse and D. Joubert, Efficiency of ab-initio total energy calculations for metals and semiconductors using a plane-wave basis set, Phys. Rev. B 59, 1758 (1999).

[18] P. E. Blöchl, Projector augmented-wave method. Phys. Rev. B 50, 17953 (1994).

[19] D. Hobbs, G. Kresse, and J. Hafner, Fully unconstrained noncollinear magnetism within the projector augmented-wave method. Phys. Rev. B 62, 11556 (2000).

[20] J. P. Perdew, K. Burke, and M. Ernzerhof, Generalized Gradient Approximation Made Simple. Phys. Rev. Lett. 77, 3865 (1996).

[21] Pui-Wai Ma and S. L. Dudarev. Constrained density functional for noncollinear magnetism. Phys. Rev. B, 91, 054420 (2015).

[22] O. Hellman, I. A. Abrikosov, and S. I. Simak, Lattice dynamics of anharmonic solids from first principles, Phys. Rev. B 84, 180301(R) (2011).

[23] N. Shulumba, O. Hellman, and A. J. Minnich, Intrinsic localized mode and low thermal conductivity of PbSe, Phys. Rev. B 95, 014302 (2017).

[24] N. Shulumba, O. Hellman, and A. J. Minnich, Lattice Thermal Conductivity of Polyethylene Molecular Crystals from First-Principles Including Nuclear Quantum Effects, Phys. Rev. Lett. 119, 185901 (2017).

[25] I. Errea, M. Calandra, and F. Mauri, Anharmonic free energies and phonon dispersions from the stochastic self-consistent harmonic approximation: Application to platinum and palladium hydrides, Phys. Rev. B 89, 064302 (2014).

[26] Alex Zunger, S.-H. Wei, L. G. Ferreira, and James E. Bernard. Special quasirandom structures. Phys. Rev. Lett., 65, 353–356, (1990).

[27] Nina Shulumba, Olle Hellman, Zamaan Raza, Björn Alling, Jenifer Barrirero, Frank Mücklich, Igor A. Abrikosov, and Magnus Odén. Lattice vibrations change the solid solubility of an alloy at high temperatures, Phys. Rev. Lett. 117, 205502, (2016).

[28] Ambroise van Roekeghem, Jesús Carrete, and Natalio Mingo, Anomalous thermal conductivity and suppression of negative thermal expansion in ScF_3, Phys. Rev. B 94, 020303(R) (2016).

[29] Y. Endoh. Lattice dynamics in ferromagnetic invar alloys. Journal of Magnetism and Magnetic Materials, 10, 177 – 182 (1979).

[30] E. D. Hallman and B. N. Brockhouse. Crystal dynamics of nickel–iron and copper–zinc alloys. Canadian Journal of Physics, 47, 1117–1131 (1969).

[31] E. Maliszewski and S. Bednarski, Lattice dynamics of $Fe_{0.65}Ni_{0.35}$ classical Invar, Physica Status Solidi (b), 211, 621–629 (2019).

[32] M. Hayase, M. Shiga and Y. Nakamura, Spontaneous volume magnetostriction and lattice constant of face-centered cubic Fe-Ni and Ni-Cu alloys, J. Phys. Soc. Jap. 34, 925 (1973).

[33] K. Hayashi and N. Mori, Effects of pressure on magnetization of Fe-Ni and Fe-Pt invar alloys, Solid State Communications, 38, 1057–1059, (1981).

[34] J. P. Rueff, A. Shukla, A. Kaprolat, M. Krisch, M. Lorenzen, F. Sette, and R. Verbeni, Magnetism of Invar alloys under pressure examined by inelastic x-ray scattering, Phys. Rev. B, 63, 132409 (2001).

[35] L. Nataf, F. Decremps, and J. C. Chervin, O. Mathon and S. Pascarelli, J. Kamarád, F. Baudelet, A. Congeduti, and J. P. Itié, High-pressure magnetic study of Fe-Ni and Fe-Pt Invar alloys, Phys. Rev. B 80, 134404 (2009).

[36] J. Kamarád, M. Míšek, and Z. Arnold, Direct measurement of magnetization isotherms of $Fe_{64}Ni_{36}$ Invar alloy in a diamond anvil cell, High Pressure Research 34, 365 (2014).

[37] I. Seki and K. Nagata, Lattice Constant of Iron and Austenite Including Its Supersaturation Phase of Carbon, ISIJ International 45, 12 (2005)

[38] We have estimated the error in the pressure calculations to be roughly a few kbar, thus qualitatively validating the finding that the points a and c in the left panel of Fig. 4 are consistent with near-zero thermal expansion in Invar.

[39] F. C. Nix and D. MacNair, The thermal expansion of pure metals: Copper, Gold, Aluminum, Nickel, and Iron, Phys. Rev. 60, 597 (1941).

[40] E. F. Wasserman. *Ferromagnetic materials: a handbook on the properties of magnetically ordered substances*, volume 5, chapter Invar, pages 237–322. North-Holland, Amsterdam, (1990).